Electronic Supplementary Material (ESI) for Journal of Materials Chemistry A.

Electronic Supplementary Information

An extremely transparent and multi-responsive healable hydrogel strain sensor

Min Wang, Hong Chen, Xiaoxia Li, Guokai Wang, Can Peng, Wen Wang, Fan Zhang, Jianqing Wang, Huanhuan Liu, Guoqing Yan*, Haili Qin**

EXPERIMENTAL SECTION

Materials. Acrylamide (AM, Aladdin, ≥98%), N, N'-bis(acryloyl)cysteamine (BACA, Alfa Aesar, 98%), Potassium peroxydisulfate (KPS, Aladdin, 99.99%), Catechin (Chem Faces, ≥98%), Carboxyl multiwalled CNTs (c-MWCNTs, XFNANO), 3-(4,5-dimethylthiazol-2-yl)-2,5-diphenyltetrazolium bromide (MTT, Alfa Aesar, 98%), Human hepatic cell line (QSG, Shanghai Institute of Cell Biology). All the above reagents were used without further purification. All the water mentioned in this work was Milli-Q purified water.

Preparation of CCMP hydrogel. CCMP hydrogel was prepared by polymerizing monomer of AM, crosslinker of BACA, initiator of KPS, in the presence of desired content of c-MWCNTs and self-assembled catechin nanoparticles (CNPs). Specifically, 2.5 mg of catechin was in the aqueous solution and c-MWCNTs with different amounts was added and further ultrasonicated for 30 min to fabricate the catechin modified c-MWCNTs. Then, 1 g of AM, 3 mg of BACA and 15 mg of KPS were added to the above solution. Before polymerization, the mixture was bubbled with N_2 for 10 min to eliminate the O_2 dissolved in the above solution. Subsequently, the above mixture was placed into an oven at 60 ^oC for 6 h to fabricate the final CCMP hydrogel. To systematically investigate the influence of catechin nanoparticles and c-MWCNTs, series of control samples including PAM, PAM/CNPs, PAM/c-MWCNTs hydrogels were also fabricated. In detail, PAM hydrogel was prepared by the polymerizing monomer of AM, crosslinker of BACA, initiator of KPS. PAM/CNPs and PAM/c-MWCNTs hydrogels were prepared the same as the PAM hydrogel except the introduction of CNPs and c-MWCNTs, respectively.

Mechanical performances. The mechanical behavior of hydrogels was carried out on a tensile machine at room temperature. Typically, the hydrogel was cut into a rectangular shape with a length of 20 mm, a width of 8 mm, a thickness of 2 mm and fixed with the plexiglass clamps. The stretch rate was controlled at a constant value of 100 mm/min. The tensile stress was determined as the force multiplied by the ration of the real-time length between the clamps and the initial length of the sample. And the strain was defined as the deformed length divided by the initial length of the samples. The toughness was calculated from the area covered by the tensile stress-strain curve. The elastic modulus was obtained from the slope of the stress–strain curve at a strain of 200%.

Adhesion performance. The tissue adhesiveness of the hydrogels was characterized by a tensile-adhesion test using porcine skin to mimic the natural tissue on a tensile machine (Instron 5565A). The hydrogels were adhered to the porcine skin with a bonded area of 25 mm × 8 mm. Then the samples were separated from the porcine skin by a tensile machine at the speed of 5 mm/min. The adhesion strength was calculated by the measured maximum strength divided by the bonded area. The different substrate materials included PP, Wood, PTFE, Rubber, Ceram, PE, and Al.

Conductivity measurements and sensing analysis. The conductivity measurements were performed on hydrogels of a diameter of 25 mm and a thickness of 4 mm and R was the resistance (Ω), U was the circuit potential (V) and I was the current corresponding (A), using digital multi-meter (DMM). The hydrogel thickness in cm, the electrode area in cm2 and resistance in Ω were L, A and R, respectively. The resistance and conductivity were defined by the following equation: $R = U / I$; $\sigma = L / R \times A$. Strain sensing experiments were measured on

CHI760E electrochemical workstation at 0.1 V constant voltage. The length, width and height of samples were 35 mm, 5mm and 2 mm. R_0 and R_s were the resistance without strain and with applied strain, respectively. The relative resistance change ($\Delta R/R_0$) was calculated by the following equation: $\Delta R/R_0 = (R_s - R_0)/R_0$. The strain sensitivity of the sensor was calculated by gauge factor (GF). The value of GF was demoted by the following formula: $GF = (\Delta R/R_0) / \varepsilon$, where ε is the strain.

Transmittance test. The transmittance of hydrogel was measured by UV-vis spectrophotometer. Hydrogels were cut into 20 mm×20 mm×2 mm slices and placed on glass slides. The transmittance of hydrogel at 400 nm to 800 nm wavelength was measured in transmittance mode of ultraviolet spectrophotometer.

Self-healing performance. Before the healing procedure, hydrogels ($20\times8\times2$ mm^3) were cut into two equal lengths along the cross-section, which were brought into contact close in a vial. Then these hydrogel surfaces were brushed with acid solution of HCl (1 mol/L) and self-healed for 24 h in the low pH-induced process. Microwave induced-healing procedure was conducted in the microwave oven for healing. After self-healing, tensile and reloading tests were carried out to evaluate their stretchability and loading capacity.

In vitro biocompatibility investigation. The cytotoxicity of hydrogels was evaluated by MTT assay. Briefly, the sterilized hydrogel samples were immersed into Dulbecco's modified eagle medium (DMEM) for the preparation of hydrogel extracts. Subsequently, QSG cells (4×10^3 cells/well) were seeded in a 96-well plate and incubated with different hydrogel extracts at 37 °C, respectively. After 24 h, the cell morphology was observed by optical microscope. Then,

the cells were sequentially co-cultured with MTT soluton (0.5 mg/mL) for another 4 h, washed three times using PB, and immersed in DMSO (150 μL). Finally, the absorbance was measured at 570 nm by a microplate reader.

Characterization. A field-emission scanning electron microscope (Zeiss Merlin Compact, Germany) equipped with an Oxford Inca energy instrument at an accelerating voltage of 5 kV was used to obtain SEM images. TEM was measured on a Hitachi H7700 transmission electron microscopy at an acceleration voltage of 120 kV. The mechanical experiments and adhesive test were carried out using a Instron 5565A tensile tester. The absorption spectra were obtained on a UV-vis spectrophotometer (UV-2600, SHIMADZU).

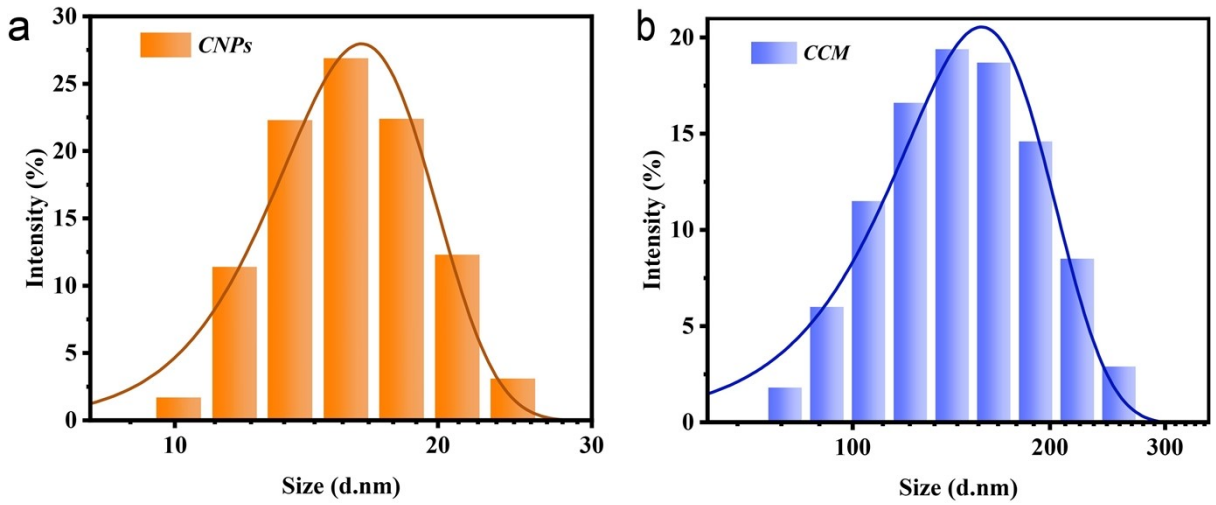

Fig. S1. Size distribution of (a) CNPs and (b) CCM nanoparticles.

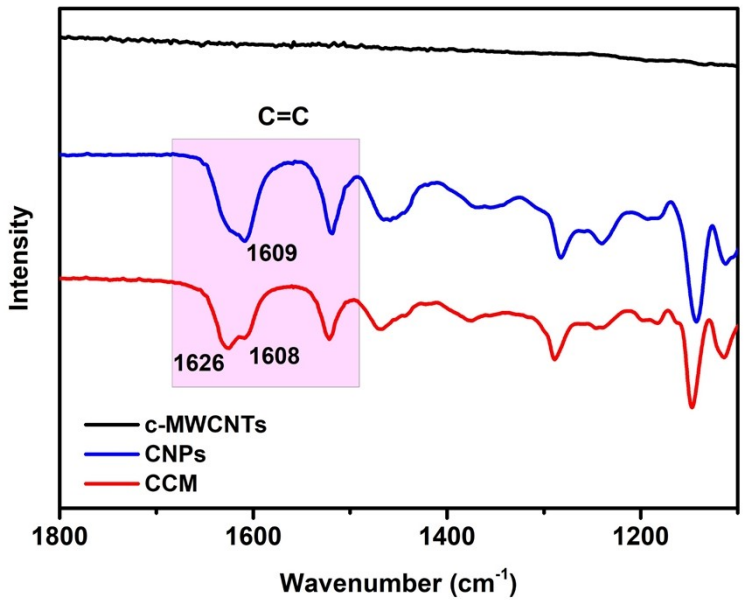

Fig. S2. FT-IR spectra of c-MWCNTs, CNPs and CCM.

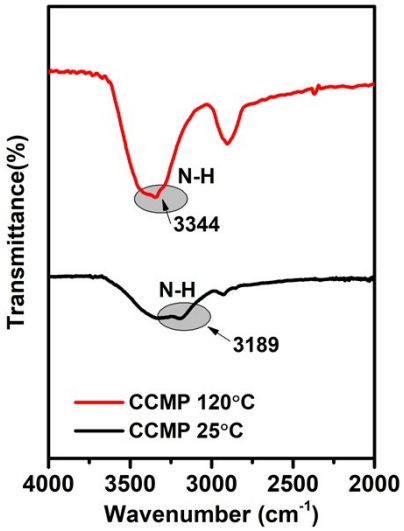

Fig. S3. Variation temperature FT-IR spectra of the CCMP hydrogel.

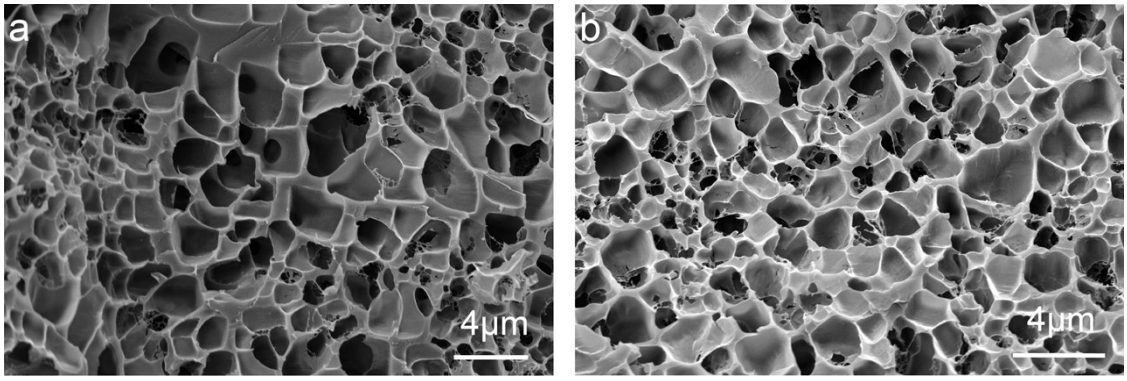

Fig. S4. SEM images of the freeze-dried (a) PAM; (b) PAM/CNPs hydrogels.

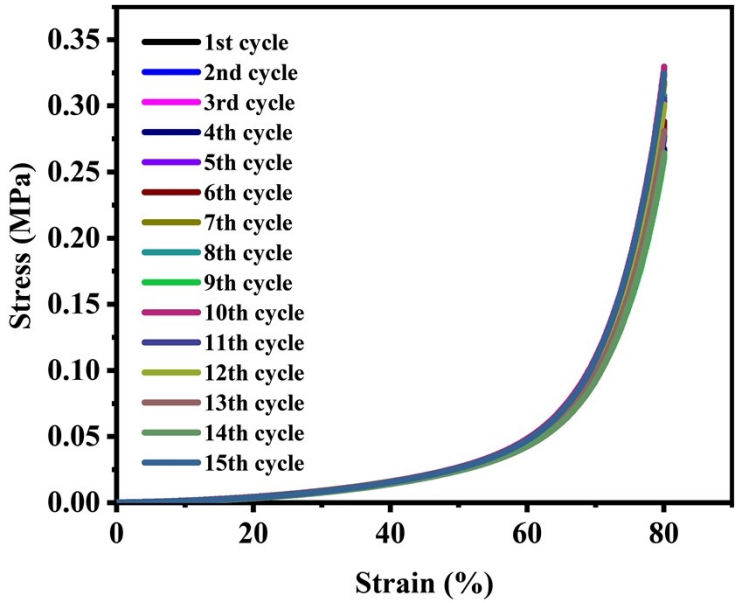

Fig. S5. Successive cyclic compressive curves of CCMP.

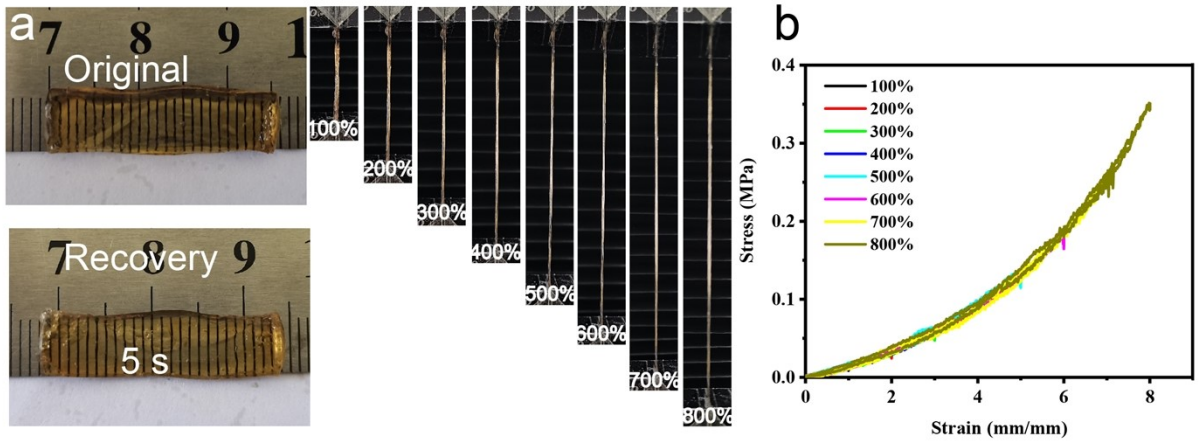

Fig. S6. (a) Optical images showing the self-recovering process of CCMP hydrogel. (b) Tensile stress-strain curves of CCMP hydrogels subjected to loading and unloading to measure hysteresis.

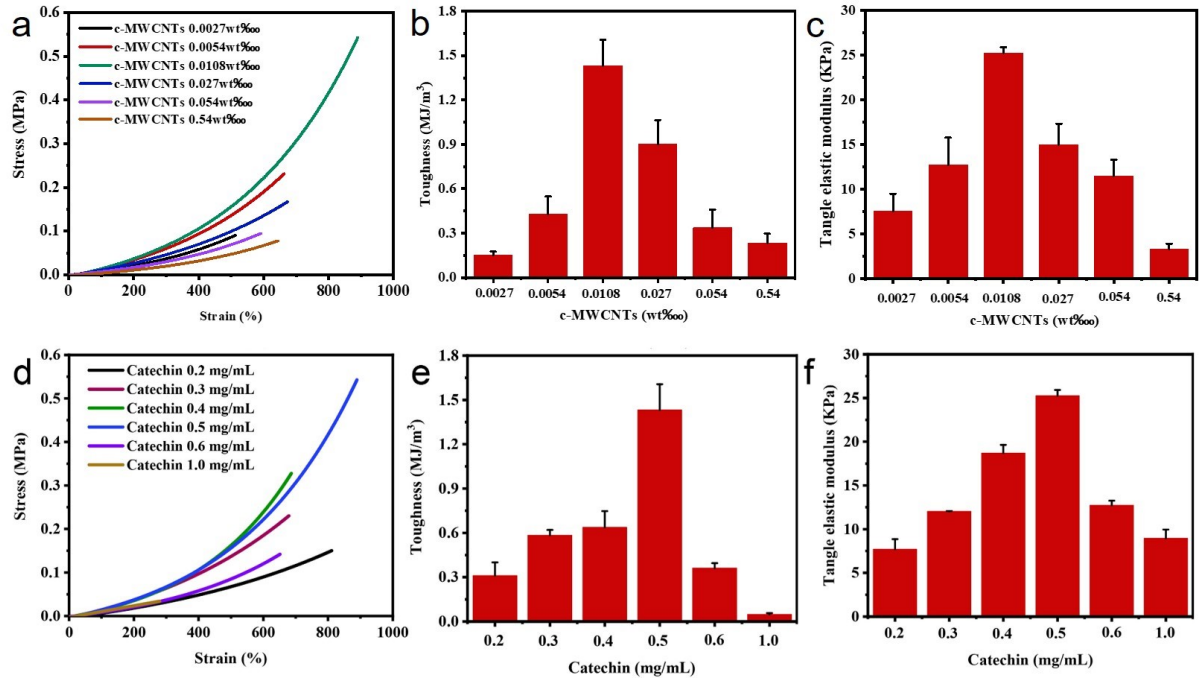

Fig. S7. (a) Tensile stress-strain curves, (b) toughness and (c) tangle elastic modulus of CCMP hydrogels with different content of c-MWCNT. (d) Tensile stress-strain curves, (e) toughness and (f) tangle elastic modulus of CCMP hydrogels with different content of catechin.

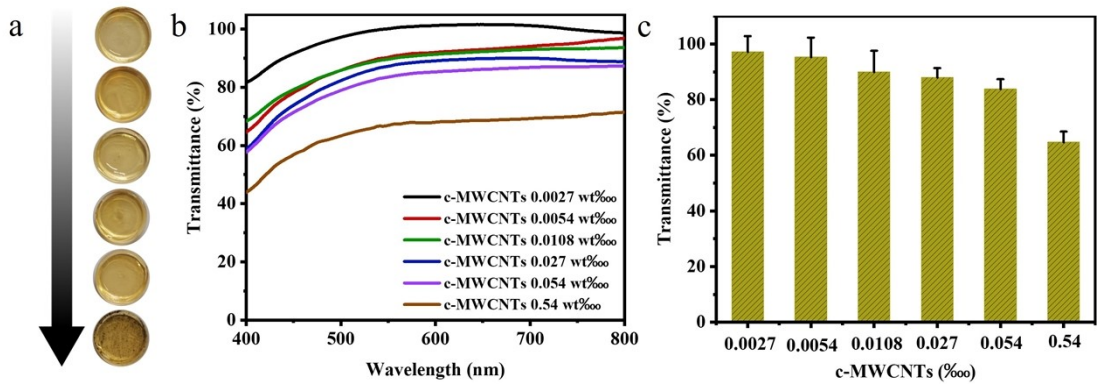

Fig. S8. (a) Optical images and (b) transmittance spectra of CCMP hydrogels with increasing content of CNTs. (c) Transmittances of CCMP hydrogels with different CNT content at 550 nm (visible region).

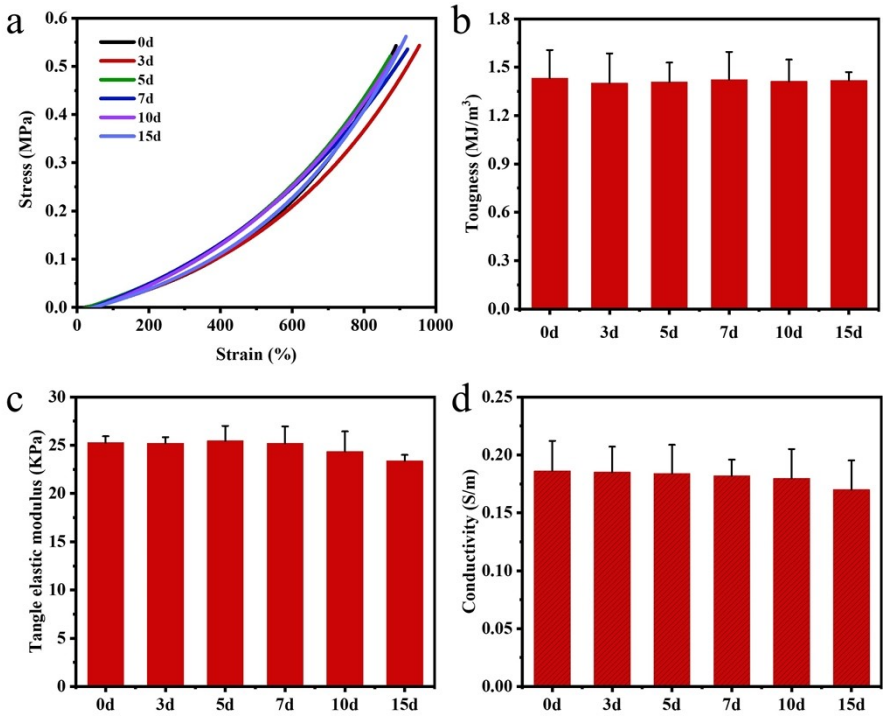

Fig. S9. (a) Stress-strain curves of CCMP hydrogel as a function of time. (b) Toughness, (c) tangle elastic modulus and (d) conductivity values of CCMP hydrogels as a function of time.

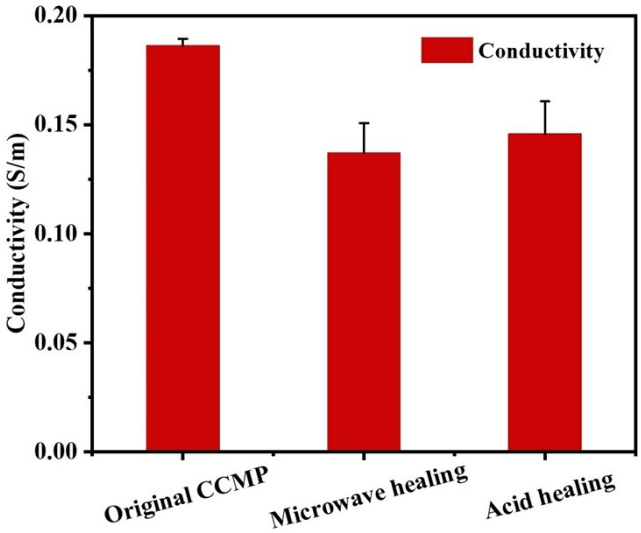

Fig. S10. Electronic conductivity of the original CCMP hydrogel and healed samples under the condition of microwave and acid.

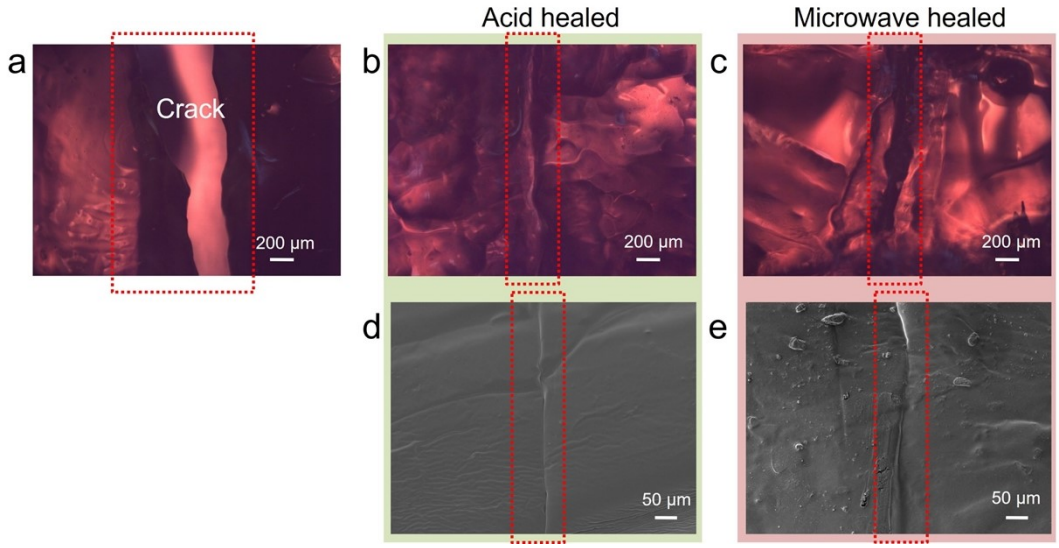

Fig. S11. Optical images showing the micromorphological changes between (a) original and healed samples after (b) acid and (c) microwave treatments. SEM images showing the healed interfacial structure.

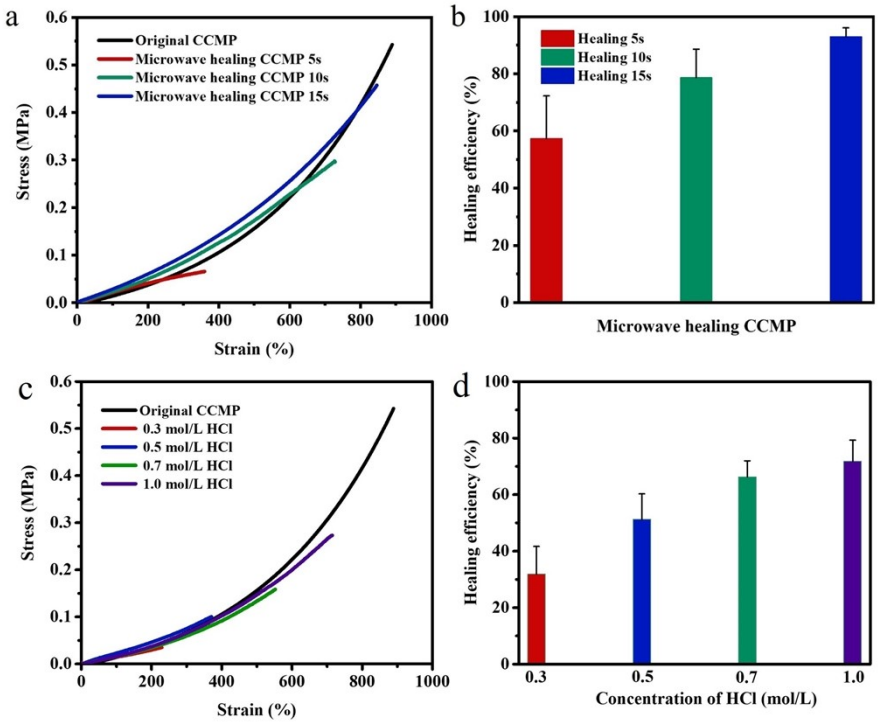

Fig. S12. (a) Stress-strain curves and (b) healing efficiency of healed CCMP hydrogel at different healing times under microwave irradiation relative to its original sample. (c) Stress-strain curves and (d) healing efficiency of healed CCMP hydrogel at different concentration of HCl in the self-healing process relative to its original sample.

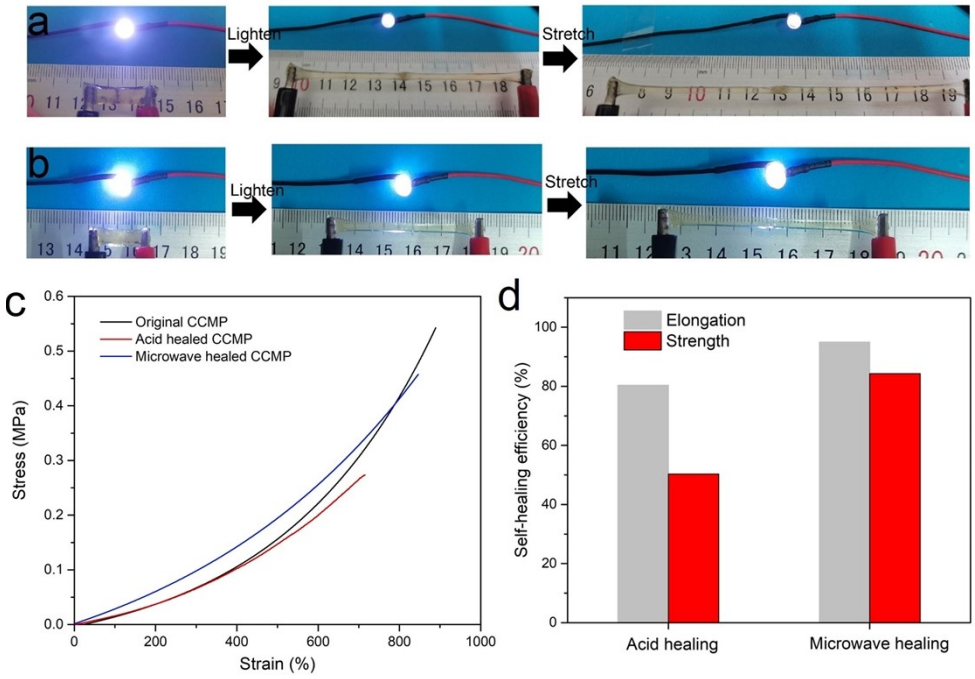

Fig. S13. Optical images show the excellent healing ability of CCMP hydrogel under different stimuli of (a) microwave, (b) acid. (c) Stress-strain curves of original CCMP and its healed samples with diverse conditions (d) Self-healing efficiency of CCMP hydrogel in terms of elongation and strength under the conditions of microwave and acid.

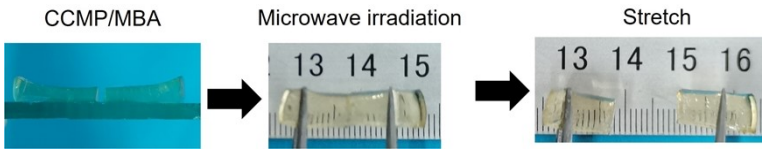

Fig. S14. Optical images showing the self-healing experiment of control sample, CCMP/MBA hydrogel.

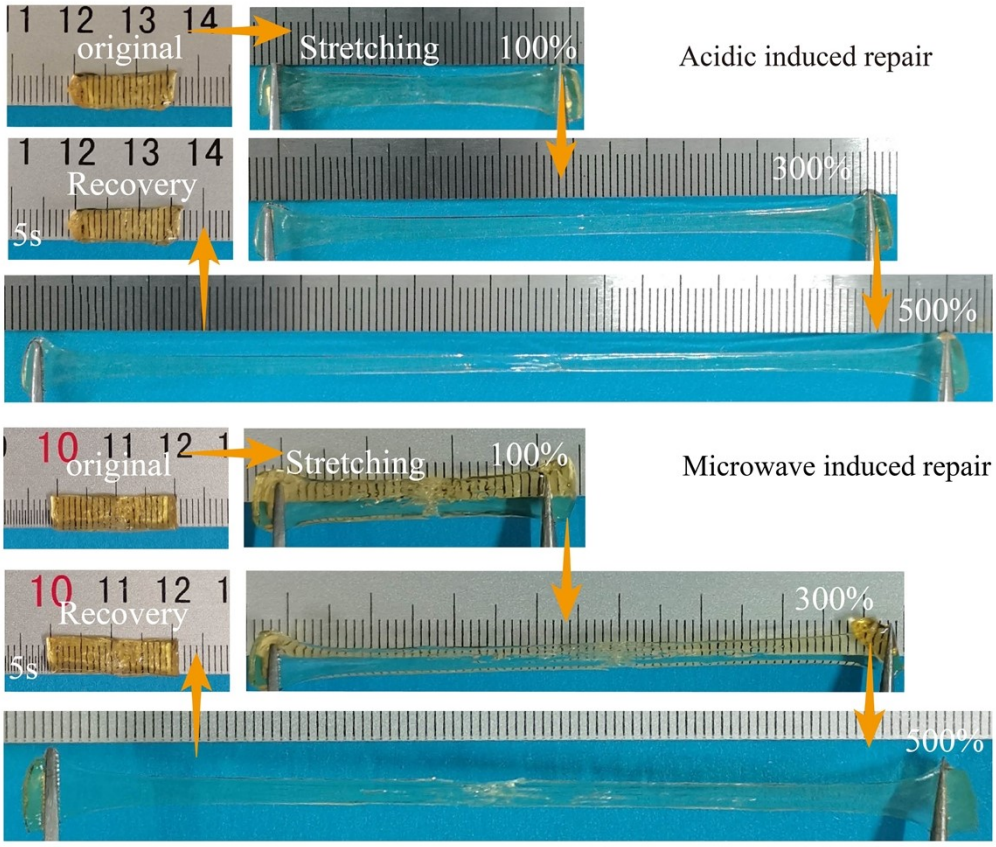

Fig. S15. Optical images showing the stretching and self-recovering process of repaired CCMP hydrogel.

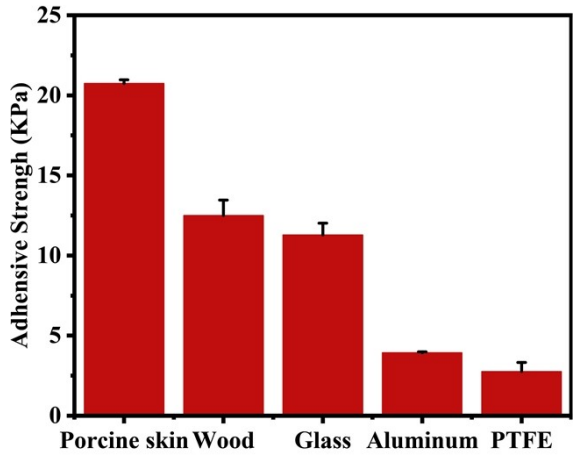

Fig. S16. Adhesion strength of the CCMP hydrogel to different substrates.

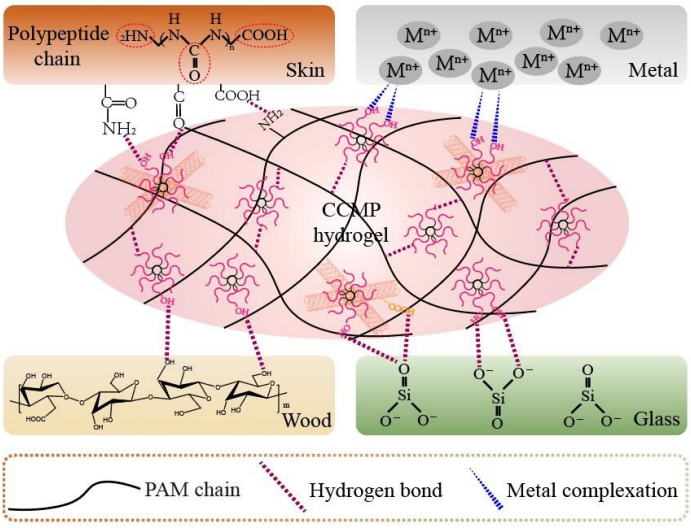

Fig. S17. Schematic illustration of adhesion mechanism of CCMP hydrogel with different substrates.

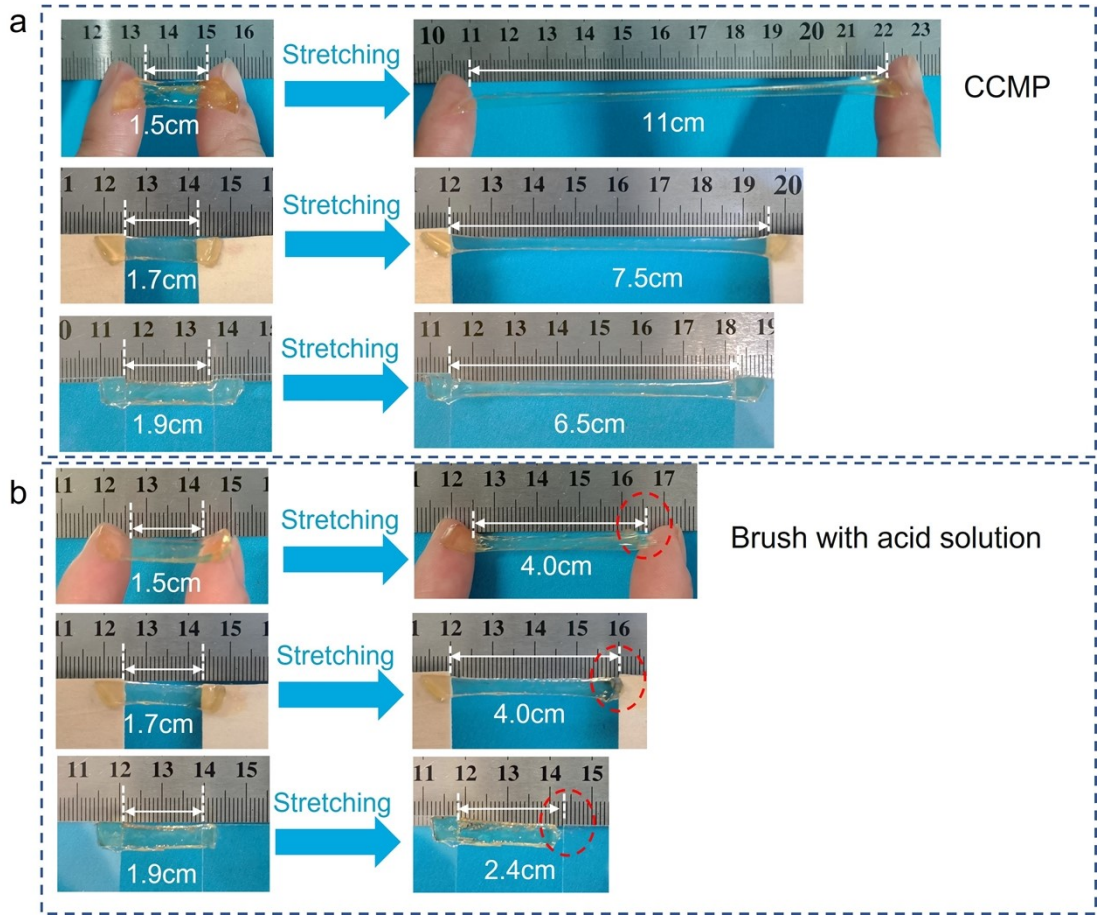

Fig.S18. Optical images showing the contribution of hydrogen bonding on strong adhesion with materials of skin, wood and glass.

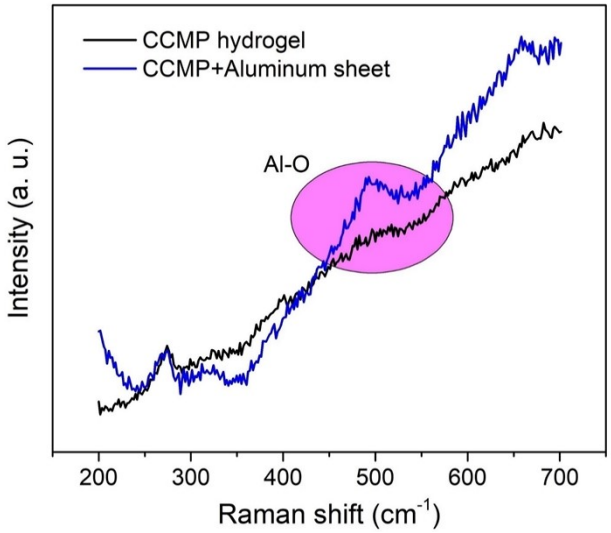

Fig. S19. Raman spectra of the CCMP hydrogel and CCMP adhered on the Aluminum sheet.

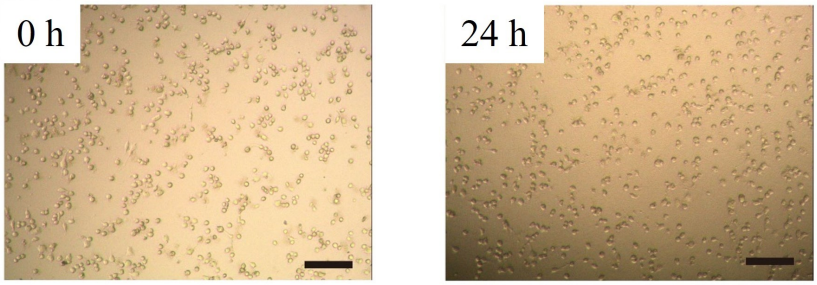

Fig. S20. Control experiment of the *in vitro* cell cytotoxicity investigation. Scale bar = 100 μm.

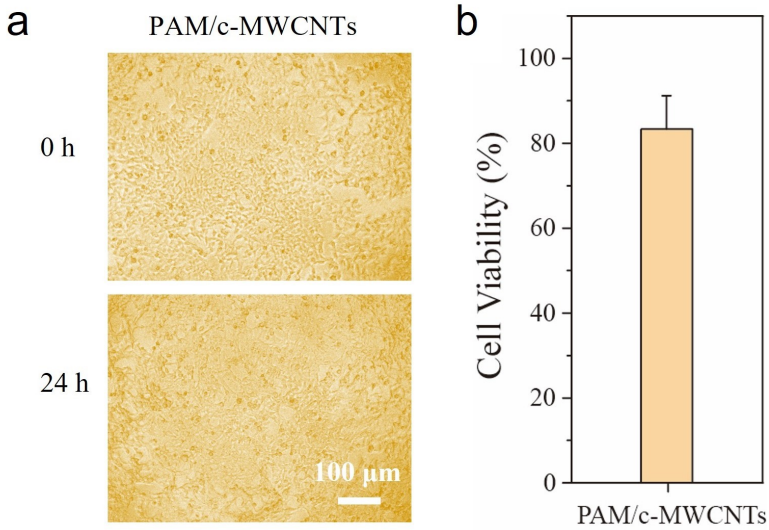

Fig. S21. (a) Microscopy images of cells co-cultured with PAM/c-MWCNTs hydrogel for 0 and 24 h, respectively. (b) Cytotoxicity of cells co-cultured with PAM/c-MWCNTs hydrogel after 24 h determined by MTT assay.

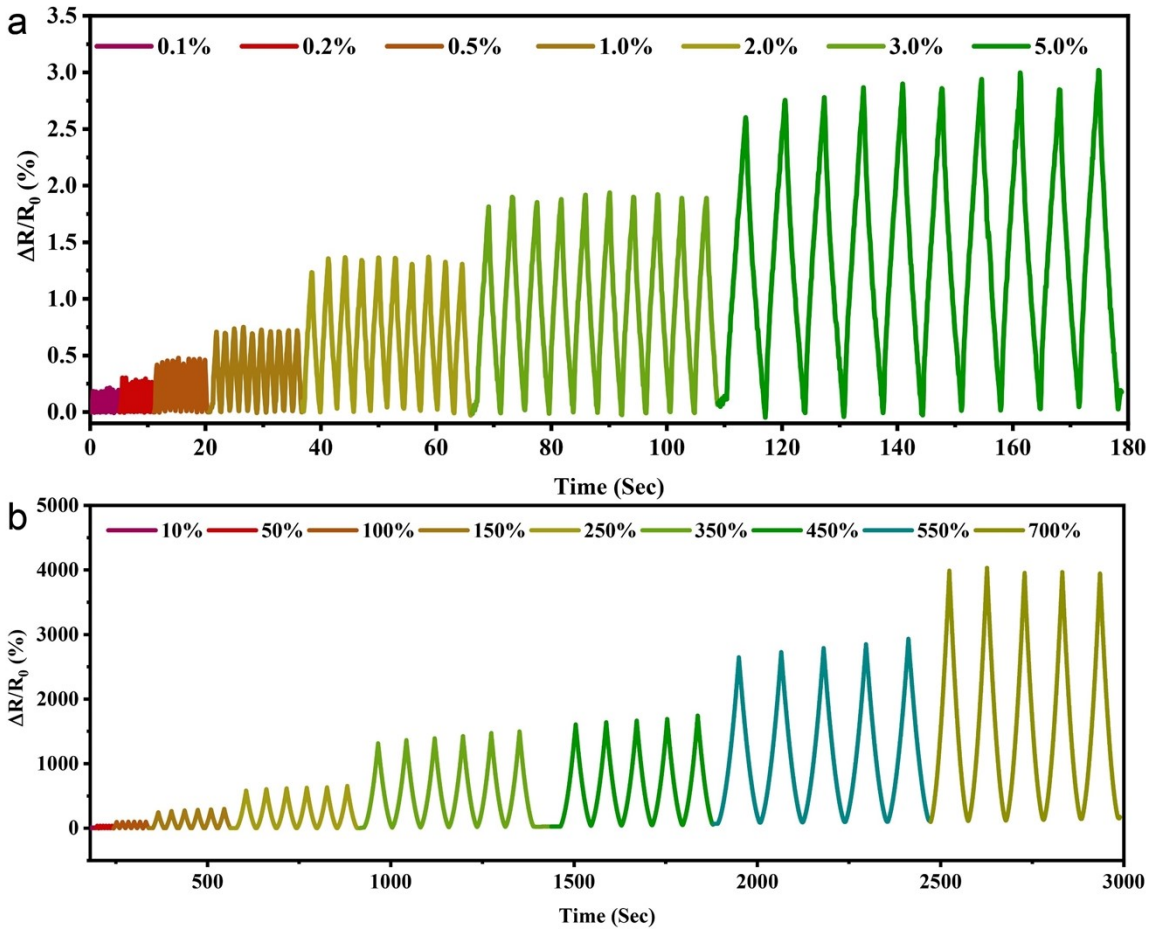

Fig. S22. $\Delta R/R_0$ versus time for CCMP hydrogel sensors with (a) small and (b) large strains.

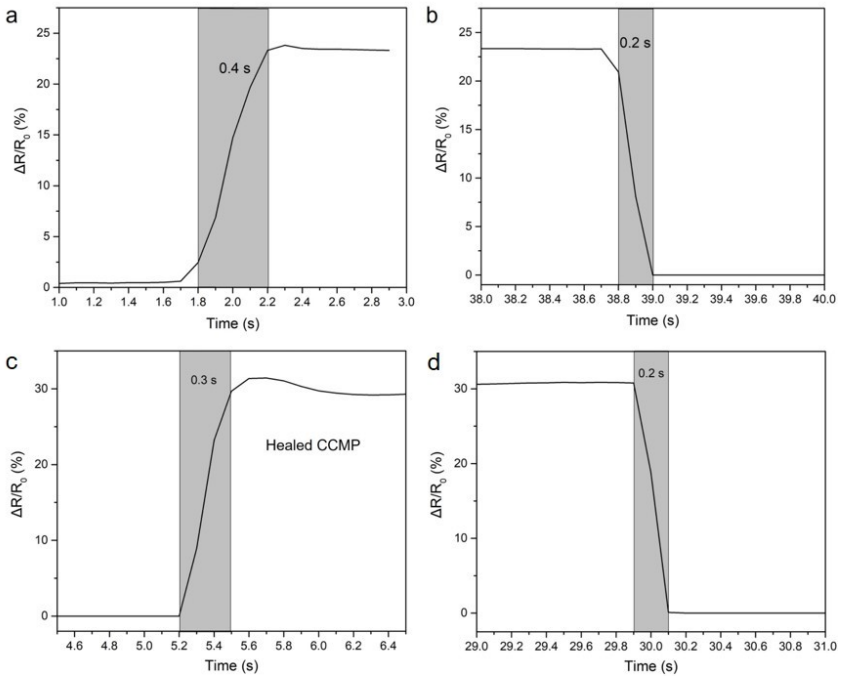

Fig. S23. The response time of (a-b) CCMP hydrogel sensor and (c-d) healed sample.

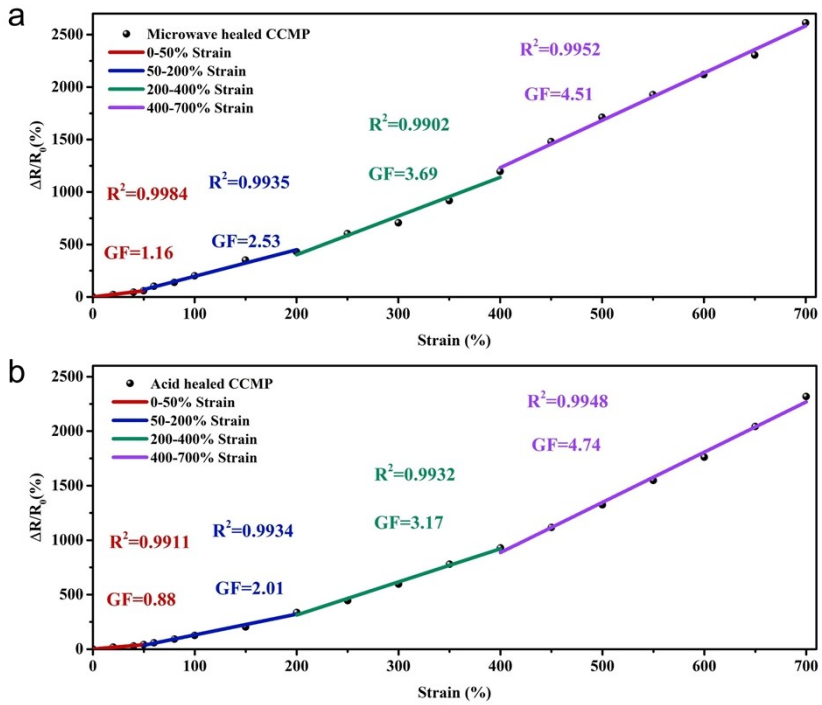

Fig. S24. $\Delta R/R_0$-strain curve of healed CCMP hydrogel under the condition of microwave and acid.

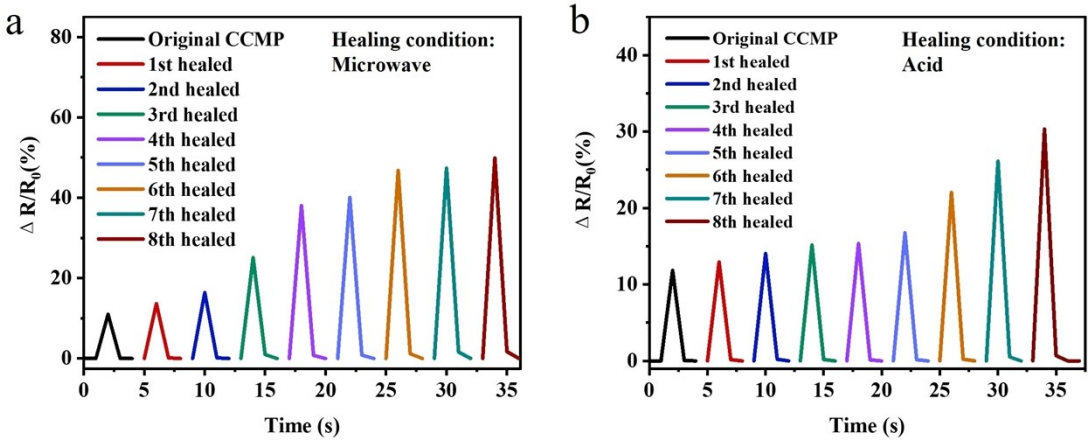

Fig. S25. $\Delta R/R_0$ versus time of the CCMP hydrogel sensor in the (a) acid- and (b) microwave-induced healing process over successive cutting-healing process.

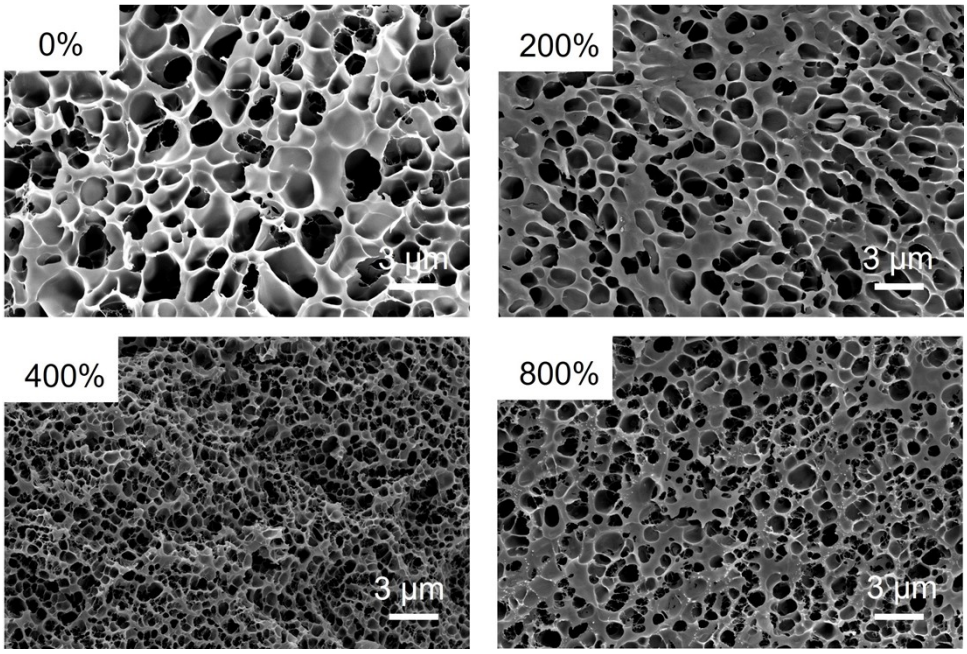

Fig. S26. SEM images of the freeze-dried CCMP hydrogels under different strains.

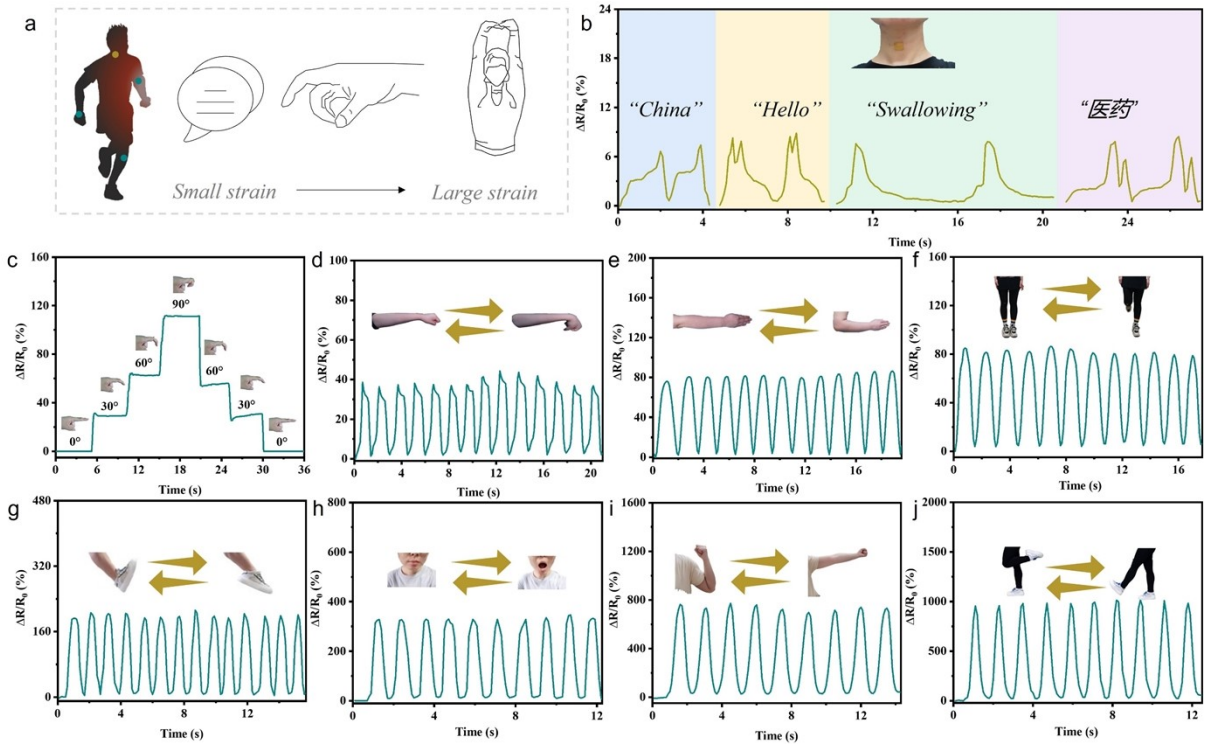

Fig. S27. Healed CCMP hydrogel as wearable sensors to monitor the human motion in different strains. (a) Schematic illustration of human motion with deformations from small to large strains. $\Delta R/R_0$ versus time for (b) phonation, (c) finger bending at different angles, (d) wrist bending (e) elbow bending, (f) knee bending, (g) ankle stretching, (h) mouth opening, (i) arm stretching and leg stretching. The inset images showing the corresponding deformations of the body.